I. D. Theodorakopoulos

DETERMINATION OF THE USEFUL FREQUENCY FOR THE CALCULATION OF THE ATTENUATION COEFFICIENT AND PHASE VELOCITY IN A VISCOELASTIC HOPKINSON PRESSURE BAR

Manufacturing Technology Division, Department of Mechanical Engineering, National Technical University of Athens, 9 Iroon Polytechniou, 15780, Athens, Greece. Email: john_theodorakopoulos@instron.com

Abstract. The propagation coefficient associated with the wave dispersion and attenuation in viscoelastic bars is calculated experimentally. The phase velocity and the attenuation coefficient in relation to the frequency are obtained from a series of impact tests on a PMMA Hopkinson pressure bar using ball bearing projectiles of different diameters. A wave dispersion correction technique is applied using the Fast Fourier Transforms of the longitudinal strains associated with the incident and reflected waves.

Key words*:* viscoelastic Hopkinson pressure bar, attenuation coefficient, phase velocity, FFT wave dispersion correction technique.

1. Introduction.

The stress wave propagation in linear elastic or viscoelastic bars is studied in various experimental techniques, such as the split Hopkinson pressure bar method, which is used to determine the dynamic/impact behaviour of materials at high strain rates. The Split Hopkinson Pressure Bar (SHPB) apparatus was brought to maturity in 1949 by Kolsky [1]. It consists of two long uniform cylindrical pressure bars, known as the incident and transmitter bars, and a short specimen sandwiched between them. A compressive pulse is produced by the impact of a striker bar (projectile) at the free end of the input bar. The projectile is fired at the input bar at various velocities, producing this way a rectangular pulse. When the pulse reaches the specimen, part of it is reflected back to the input bar, while the remaining pulse is transmitted to the output bar. The amplitude of the transmitted and reflected waves depends on the impedance mismatch between the specimen and the pressure bars. The three waves, incident, reflected and transmitted $[\varepsilon_I(t), \varepsilon_R(t), \varepsilon_T(t)]$ are picked up by a pair of strain gauges located usually at the mid-point of each bar. The gauges are connected to a Wheatstone bridge station, and the signals after they have been amplified, they are converted to force-time pulses using a data logger. Since the conventional SHPB apparatus was designed to employ linear elastic steel bars of high mechanical impedance, the use of specimens made of low density cellular materials would lead to errors in the experimental measurements [2]. A different arrangement of the SHPB system made of a lower impedance PMMA material was successfully used to minimise these errors. In this current study the wave attenuation and phase velocity of the pulses produced by the impact of a ball bearing projectile to a strain gauged PMMA Hopkinson bar are reported.

2. Theoretical considerations.

The conventional SHPB apparatus uses linear elastic pressure bars and the dispersion of the waves that propagate in the bars will not lead to important errors; therefore, the strains measured by the gauges can be shifted to the specimen-bar interfaces in order to calculate

the three waves $[\varepsilon_I(t), \varepsilon_R(t), \varepsilon_T(t)]$ and, consequently, to determine the force and particle velocity at the end of each bar using the following relationships:

$$F_{in}(t) = E \cdot A \cdot [\varepsilon_I(t) + \varepsilon_R(t)]; \tag{1}$$

$$F_{out} = E \cdot A \cdot \varepsilon_T(t); \tag{2}$$

$$V_{in} = C \cdot [\varepsilon_I(t) - \varepsilon_R(t)]; \tag{3}$$

$$V_{out} = C \cdot \varepsilon_T(t), \tag{4}$$

where, following the notation, A is the cross-sectional area of the bars, E the Young's modulus of the material and C the stress wave velocity.

Studies have showed that, in the case of dynamic testing of cellular materials and generally materials of low mechanical impedance, the classical SHPB method is inaccurate [3, 4]. From equations (1 – 4) it is obvious that, knowledge of the output force and velocity requires only an accurate measurement of the strain imposed to the specimen by the transmitted wave. Additionally, the input force and velocity cannot be determined with any degree of confidence, if the mechanical impedance of the sample is very small in comparison to the mechanical impedance of the pressure bars. As a result of this mismatch, the majority of incident wave is reflected back into the input bar, resulting in a transmitted pulse of very low magnitude. In this case, the input force tends to zero, since ε_I is almost equal to $-\varepsilon_R$. Thus, for this type of materials, the use of low impedance pressure bars is essential for the accuracy of the tests.

Usually, the steel bars of the classical SHPB apparatus are replaced by PMMA (or nylon) rods. This material has been used by several researchers in dynamic tests with the SHPB and is considered to be suitable for this type of applications. The only limitation is that, due to the viscoelastic properties of the material, the wave dispersion effects are increased. However, a number of methods have been developed to include the dispersion effects into the dynamic analysis with the SHPB technique and software packages have been developed, which can perform the dispersion correction in minutes. Tests with PMMA bars showed an improvement in accuracy of about 200 times of that of the conventional steel bars [3].

Lifshitz and Leber performed the dispersion correction in the frequency domain after employing an FFT algorithm by adjusting the phase of each Fourier component [5]. They indicated that, the accuracy of the dynamic stress-strain curves depends not only on the accuracy of the predicted shapes of each individual pulse but, also, on their positions along the time axis. A number of tests with the SHPB system showed that, even a small change in the value of the stress wave velocity could cause a shift of a few microseconds in the position of the measured pulses. They reported that the main source of the oscillations in the stress-strain curves after performing the dispersion correction is this shift of the incident, reflected and transmitted pulses.

Zhao and Gary examined the importance of the dispersion effects in viscoelastic rods [6]. They suggested that, a three dimensional description of the wave propagation should be used in order to improve the accuracy of any SHPB system incorporating viscoelastic bars. The approach for the correction of the wave dispersion was based on the Pochhammer and Chree wave solution for an infinite elastic bar. Although this solution is only an approximation for a bar of finite length, it is accepted by many authors and provides accurate results when it is used with the SHPB system. The Pochhammer and Chree frequency equation in the case of viscoelastic bars takes the following form:

$$f(\delta) = \left(\frac{2 \cdot \kappa}{a}\right) \cdot (\beta^2 - \delta^2) \cdot J_1 \cdot (\kappa \cdot a) \cdot J_1 \cdot (\beta \cdot a) - (\beta^2 + \delta^2)^2 \cdot J_0 \cdot (\kappa \cdot a) \cdot J_1 \cdot (\beta \cdot a) +$$

$$+4 \cdot \delta^2 \cdot \kappa \cdot \beta \cdot J_1 \cdot (\kappa \cdot a) \cdot J_0 \cdot (a \cdot \beta) = 0, \tag{5}$$

where $\kappa = \frac{\rho \cdot \omega^2}{\left(\lambda^*(\omega) + 2 \cdot \mu^*(\omega)\right)} + \delta^2$, $\beta^2 = \frac{\rho \cdot \omega^2}{\mu^*(\omega)} + \delta^2$, δ is the complex change in the phase function, a is the radius of the bar, J_0 and J_1 are first order Bessel's functions and $\lambda(\omega)$, $\mu(\omega)$ are two material coefficients. Note, that, in the above equation δ is the complex change in the phase function of the angular frequency ω. The real part of ω gives the relationship between the frequency and the phase velocity and the imaginary part gives the relationship between the frequency and the damping coefficient of the bars.

To illustrate the importance of the dispersion effects they carried out tests with the SHPB using PMMA rods [6]. This material is described by a number of Voigt or Kelvin elements connected in series with a spring. The elastic component (spring) and the viscous component (dashpot) are used to simulate the viscoelastic behaviour of the polymer (PMMA). In order to determine the spring and damping constants, the waves, at two or more different points in the bar, were recorded and an identification process, based on an inverse calculation technique, was applied. Once the constants were identified the rheological model was used for the dispersion correction.

Bacon [7] presented an experimental technique based on the method used by Lundberg and Blanc [8] to determine the propagation coefficient of a viscoelastic rod. This technique is used to perform SHPB tests with viscoelastic bars by taking into account the wave dispersion and attenuation in the bars. According to this method, the propagation coefficient and the wave attenuation, which are both functions of the frequency, are calculated experimentally. Bacon used the one-dimensional theory of wave propagation in viscoelastic bars and indicated that the Pochhammer and Chree frequency equation as well as knowledge of the bar mechanical properties are not necessary.

Bacon also developed a two point strain measurement method for the separation of the waves propagating in an elastic, or viscoelastic, SHPB taking into account the wave dispersion and attenuation in the bars [9]. He performed the wave separation in the frequency and time domains and showed that the phase velocity and damping coefficient of the bars can be determined theoretically, as well as experimentally. His technique is a generalization of the Lundberg and Henchoz method, which is based on the one dimensional elastic wave propagation theory.

As mentioned above, PMMA exhibits viscoelastic behaviour, therefore, the wave attenuation and velocity in the pressure bars are both functions of the frequency.

Consider an axially impacted viscoelastic bar of length L, with a set of strain gauges mounted at $x = 0$, as schematically illustrated in Fig. 1.

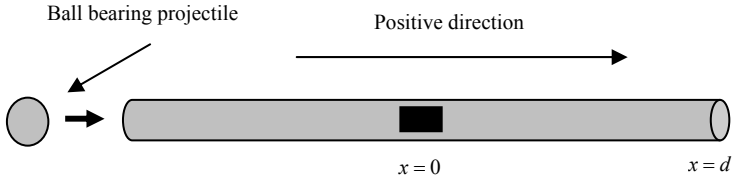

Fig. 1. Axially impacted viscoelastic rod.

According to the one-dimensional theory of wave propagation, the equation of axial motion in the frequency domain is:

$$\frac{\partial^2}{\partial x^2}\tilde{\sigma}(x,\omega) = -\rho \cdot \omega^2 \cdot \tilde{\varepsilon}(x,\omega), \tag{6}$$

where, $\tilde{\sigma}(x,\omega)$ and $\tilde{\varepsilon}(x,\omega)$ are the Fourier transforms of the stress and strain, respectively. The material is linear viscoelastic, thus, the constitutive relation between stress and strain is:

$$\tilde{\sigma}(x,\omega) = E^*(\omega) \cdot \tilde{\varepsilon}(x,\omega), \tag{7}$$

$E^*(\omega)$ is the complex Young's modulus of the material. The coefficient of the wave propagation, which is representative of the wave dispersion and attenuation in the viscoelastic bar, is defined as:

$$\gamma^2 = -\frac{\rho \cdot \omega^2}{E^*} . \tag{8}$$

Using relationships (7) and (8) the wave equation becomes:

$$\left(\frac{\partial^2}{\partial x^2} - \gamma^2 \right) \cdot \tilde{\varepsilon}(x, \omega) = 0 \tag{9}$$

and, therefore, the general solution of equation (9) is:

$$\tilde{\varepsilon}(x, \omega) = \tilde{\varepsilon}_I(\omega) \cdot e^{-\gamma \cdot x} + \tilde{\varepsilon}_R(\omega) \cdot e^{\gamma \cdot x} . \tag{10}$$

Moreover, the Fourier transform of the normal force at the cross-section x is:

$$\tilde{F}(x, \omega) = -\frac{\rho \cdot A \cdot \omega^2}{\gamma^2} \cdot \left(\tilde{\varepsilon}_I(\omega) \cdot e^{-\gamma \cdot x} + \tilde{\varepsilon}_R(\omega) \cdot e^{\gamma \cdot x} \right), \tag{11}$$

where, $\tilde{\varepsilon}_I(\omega)$ and $\tilde{\varepsilon}_R(\omega)$ are the Fourier transforms of the longitudinal strains at $x = 0$, corresponding to the incident wave and its first reflection at the free end of the bar, respectively. The propagation coefficient $\gamma(\omega)$, the phase velocity $C(\omega)$, the wave number $k(\omega)$ and the attenuation coefficient $a(\omega)$ are related as:

$$\gamma(\omega) = a(\omega) + i \cdot k(\omega) = a(\omega) + i \cdot \frac{\omega}{C(\omega)} . \tag{12}$$

Since one end of the bar is free, the normal force at that end is zero and, consequently, equation (11) becomes:

$$\tilde{\varepsilon}_I(\omega) \cdot e^{-\gamma(\omega) \cdot d} + \tilde{\varepsilon}_R(\omega) \cdot e^{\gamma(\omega) \cdot d} = 0 , \tag{13}$$

where, d is the distance between the strain gauges and the free end of the bar.

3. Experimental.

The determination of the phase velocity and the attenuation coefficient was carried out using the strain records from a series of impact tests on a PMMA bar impacted by two ball bearing projectiles of different diameters. The apparatus which was used for the experiments is shown in Fig. 2. The dimensions of the pressure bar and the projectiles, as well as the material properties, are given in Table 1.

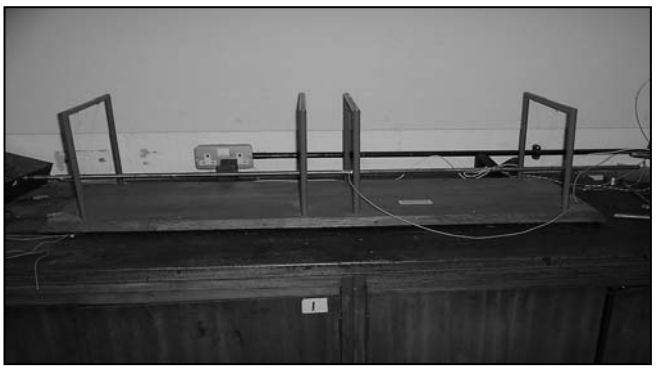

Fig. 2. Experimental set-up used for the determination of the phase velocity and attenuation coefficient.

Table 1. Projectile and pressure bar dimensions and properties

Projectile / Pressure bar types	Material	Diameter (mm)	Length (mm)	Young's modulus (GPa)	Tensile strength (MPa)	Impact strength (kJ/m^2)
Ball bearing	Silver steel	12	-	211	700	1000
Ball bearing	Silver steel	20	-	211	700	1000
Pressure bar	PMMA	20	1000	2-3	55-80	15

As shown in Fig. 2, four strings are holding the bar in such a way so it can swing freely along its axial direction. Three pairs of strain gauges were cemented on the bar at different locations; see Fig. 3, *a*, in order to examine the change in the shape of the pulse due the material damping. Note, also, that each pair of strain gauges formed the arms of a Wheatstone bridge circuit, as shown in Fig. 3, *b*.

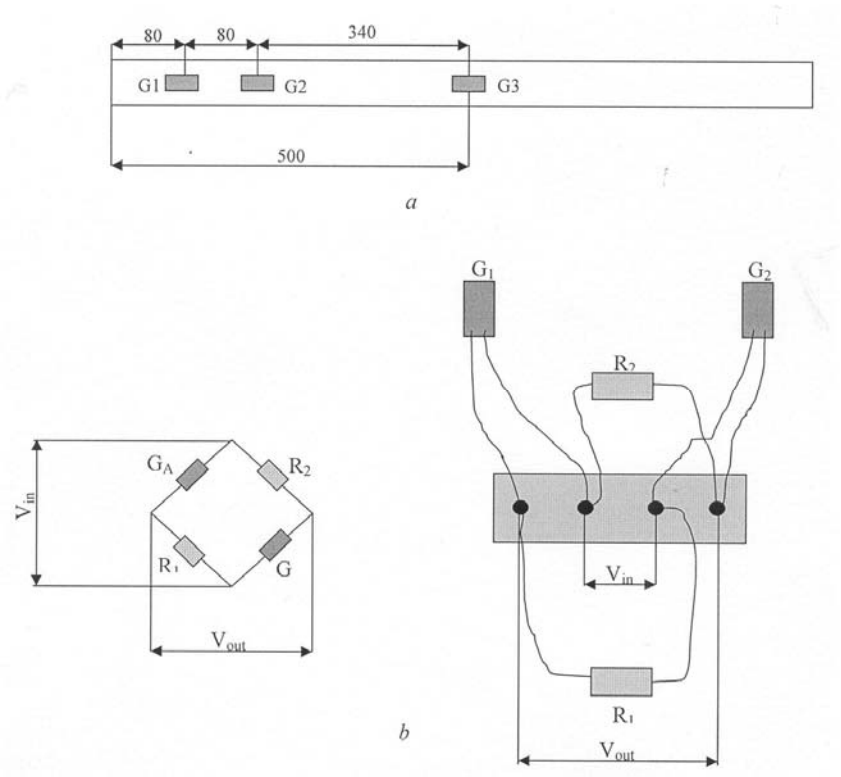

Fig. 3, a. Location of strain gauges and *b* Wheatstone bridge arrangements of the PMMA bar.

There are two active arms in the Wheatstone bridge circuit, the remaining arms are connected to two dummy resistors R_1 and R_2. G_A and G_B are the strain gauges, fixed diametrically opposite on the pressure bar, and V_{in} and V_{out} are the bridge input and output voltages. The strain gauges are sensitive only to the longitudinal strain components, while the bending effects are minimised. In this case, the measured strain is given by the following relationship:

$$\varepsilon = \frac{4 \cdot V_{out}}{S \cdot G \cdot V_{in} \cdot A_R}, \tag{14}$$

where, A_R is the number of active arms, S the gauge factor and G the gain setting of the amplifier. The signals were amplified using three amplifiers type 369-TA, manufactured by FYLDE Electronic Laboratories Limited. The data recorded from the strain gauges were captured by a data logger and the pulses were monitored and processed using a PC unit.

4. Results and discussion.

The output of the first impact test using the 12 mm diameter projectile is the voltage versus time plots shown in Figs 4, *a* – *c*.

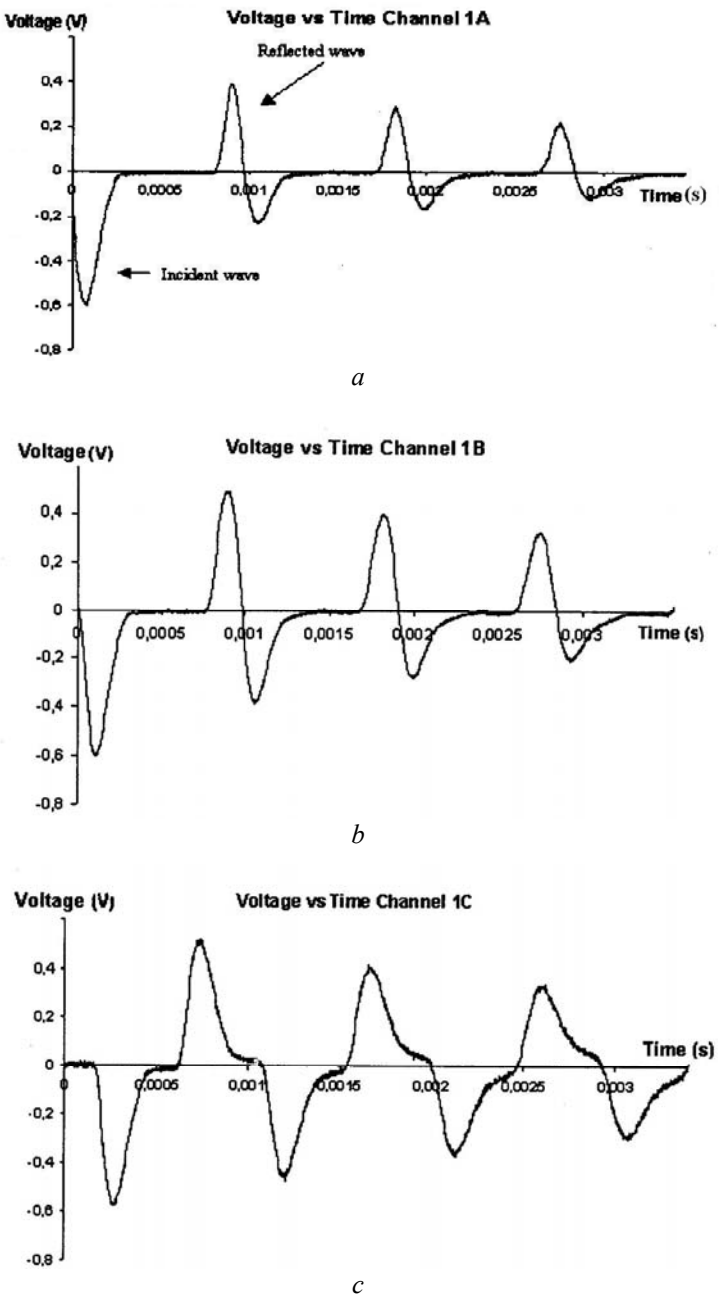

a

b

c

Fig. 4. Variation of voltage with time from the *a* first, *b* second and *c* third pair of strain gauges G_i on the pressure bar.

As shown, the stress waves generated by the impact were of triangular shape. It is obvious by observing the graphs that the level of noise increases with the distance between the point of measurement and the impacted end. Moreover, the waves, that propagate in the two directions, positive and negative, overlap at the points where the first two pairs of strain gauges are attached. Therefore, the data recorded from the third pair of strain gauges will be used in the calculations since the waves do not overlap at that point. Similar results were obtained from the impact test using the larger projectile of 20 mm diameter.

In order to perform the calculations for the phase velocity and the attenuation coefficient, the incident and reflected waves, $\varepsilon_I(t)$ and $\varepsilon_R(t)$ must be treated separately as shown in Figs 5, *a*, *b*.

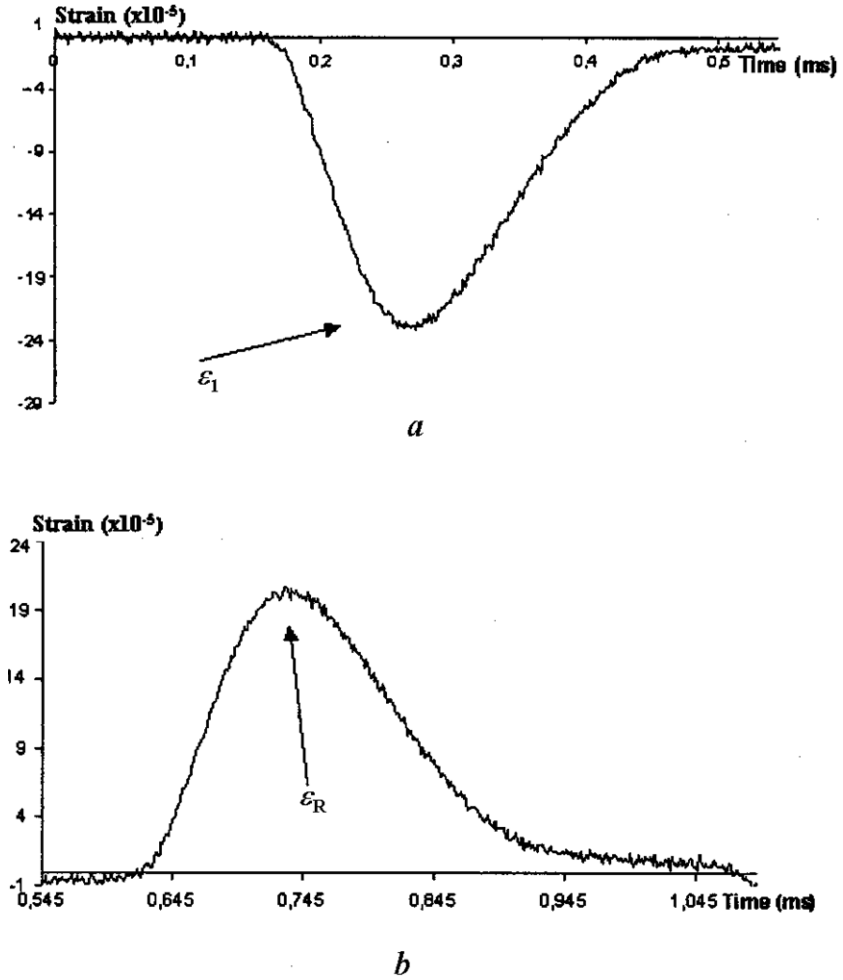

Fig. 5, a incident and *b* reflected waves.

Using equation (13) it is possible to define a transfer function $H(\omega)$, which is necessary for the calculation of the propagation coefficient, as follows:

$$H(\omega) = -\frac{\tilde{\varepsilon}_R(\omega)}{\tilde{\varepsilon}_I(\omega)} = e^{-2\cdot d\cdot\gamma(\omega)}, \tag{15}$$

where, $\tilde{\varepsilon}_I(\omega)$ is the Fourier transform of the axial strain associated with the incident pulse, which is negative (compressive wave) and, therefore equation (15) becomes:

$$\ln\left[\frac{\tilde{\varepsilon}_R(\omega)}{\tilde{\varepsilon}_I(\omega)}\right] = -2 \cdot d \cdot \gamma(\omega) \tag{16}$$

and, solving for $\gamma(\omega)$:

$$\gamma(\omega) = -\frac{1}{2 \cdot d} \cdot \ln\left[\frac{\tilde{\varepsilon}_R(\omega)}{\tilde{\varepsilon}_I(\omega)}\right]. \tag{17}$$

The attenuation coefficient can be obtained from the real part of the complex number, $\gamma(\omega)$ and the wave number from the phase of the transfer function, $H(\omega)$ after performing a numerical procedure known as unwrapping [6]. This way, the phase of the transfer function is determined in the range between 0 and 2π. Therefore, before calculating the wave number, the radian phase angle is corrected by adding multiples of $\pm 2\pi$, when absolute jumps between consecutive elements are greater than π radians. The wave number is then expressed as a monotonic continuous function of frequency. The phase velocity can be derived from equation (12) as:

$$C(\omega) = \frac{\text{Frequency}}{\text{Wave number}} = \frac{\omega}{k(\omega)}. \tag{18}$$

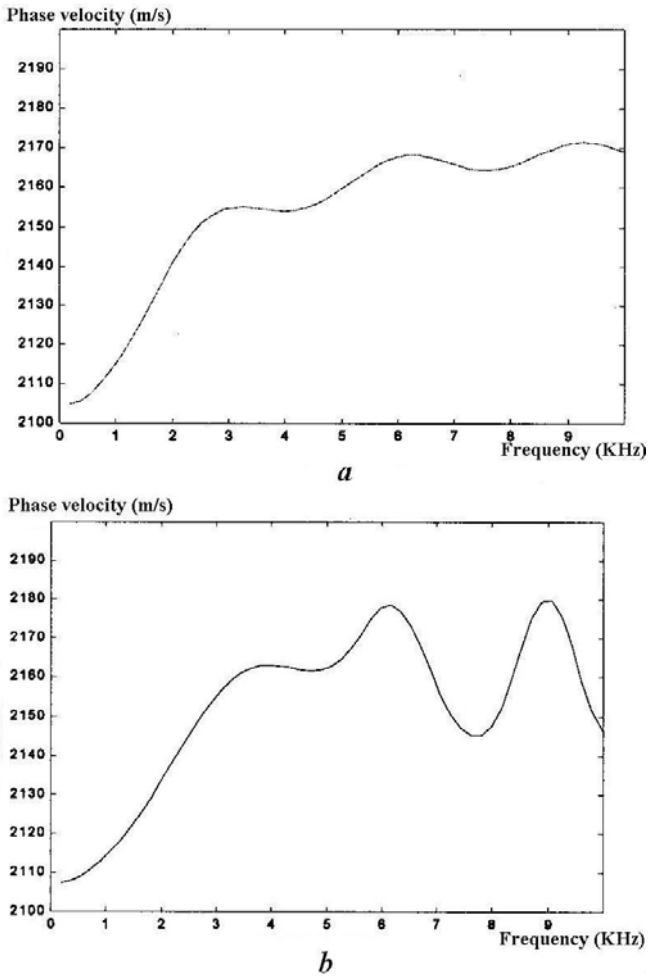

Fig. 6. Experimental phase velocity versus frequency from the impact generated by the *a* 12 mm and *b* 20 mm diameter projectiles.

The calculation of $\gamma(\omega)$, $C(\omega)$ and $a(\omega)$ was carried out using the Matlab code. After each impact test the voltage records were stored in an ASCII file. The data were sampled at 10^5 Hz and the number of points used to define the incident wave and its reflections was 29800. The voltage measurements were converted to strain using equation (14). Two double arrays were created, containing the incident and reflected waves, ε_I and ε_R. The size of these arrays, which was initially, 1×501 was increased to 1×5511, by adding a series of zeros to the strain records. This way, the phase velocity and the attenuation coefficient versus frequency curves were perfectly smooth. The values of $\tilde{\varepsilon}_I(\omega)$ and $\tilde{\varepsilon}_R(\omega)$ were then determined by taking the fast Fourier transforms of the axial strains, ε_I and ε_R, at the same time interval, from zero to 5511 microseconds. The next step was to define the transfer function $H(\omega)$, which was obtained by diving the fast Fourier transforms of the reflected and the incident waves respectively, see equation (15).

The wave number $k(\omega)$ was obtained from the phase angle of the transfer function after applying the unwrapping technique. The frequency was then defined in such a way as to include all 5511 points and the phase velocity was calculated using equation (18). Finally, the propagation coefficient, which is a complex number, was determined from the natural logarithm of the transfer function, see equation (17), and the attenuation coefficient was derived from the real part of $\gamma(\omega)$. The attenuation coefficient and phase velocity versus frequency curves obtained from the impact tests are presented in Figs 6 and 7.

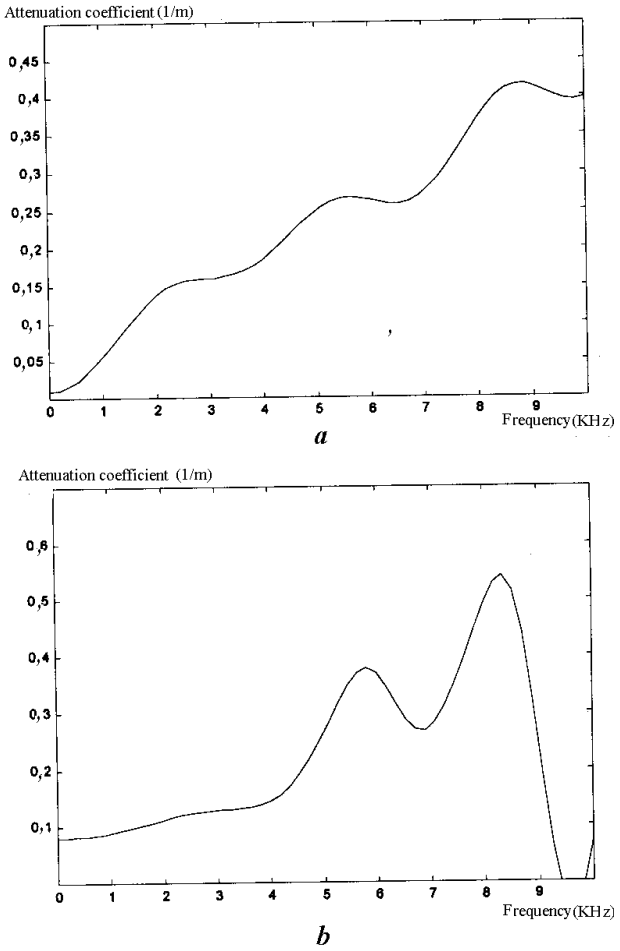

Fig. 7. Experimental attenuation coefficient versus frequency for *a* 12 mm and *b* 20 mm diameter projectiles.

The selected frequency range is 0-10 KHz, since in a typical SHPB test ω does not exceed 10 KHz. It is also important to note, that the attenuation coefficient and the phase velocity versus frequency curves for both projectiles are very close for frequencies between 0 and 5 KHz. Beyond 5 kHz the scattering increases, since the signal spectrum components become lower.

Note, also, that the fluctuations observed at higher frequencies are greater for the larger diameter projectile in which case the pulse generated by the impact is longer, compare Figs 6, *a, b* and 7 *a, b*, indicating that the accuracy of method is increased with the use of smaller projectiles. The difference in the calculated values of the phase velocity using the two projectiles for frequencies higher than 5 kHz is at maximum 2% whereas, the effect of the projectile diameter in the determination of the attenuation coefficient is much more significant. It may be observed in Fig. 7, *b*, that the attenuation coefficient curve which corresponds to the 20 mm diameter projectile drops below zero at a frequency of approximately 9,5 kHz. On the other hand, the result obtained by the strike of the 12 mm diameter projectile is very different as shown in Fig. 7, *a*, where a much smoother curve is demonstrated.

This implies that in order to study with sufficient accuracy the attenuation coefficient and phase velocity of the stress waves for the complete frequency range of a SHPB test, incorporating PMMA pressure bars, the threshold of steel projectile diameters should not exceed 12 mm. On the other hand, for projectile diameters larger than 12 mm and up to 20 mm the useful frequency range is 0 – 5 kHz.

5. Conclusions.

An experimental technique is presented for the calculation of the phase velocity and attenuation coefficient in a viscoelastic Hopkinson pressure bar by taking into account the wave dispersion effects. The longitudinal strains of the waves produced by the impact of ball bearing projectiles on the PMMA bar are measured using three pairs of strain gauges cemented at different locations on the bar. This way, the propagation coefficient, phase velocity and attenuation coefficient are determined from the Fast Fourier Transforms of the strains associated with the incident and reflected waves. Thus, C, α and γ are expressed as monotonic functions of the frequency ω.

Summarising the main features of the results reported, it may be concluded that the accuracy of this technique strongly depends on the duration of the pulse which is associated with the diameter of the projectile, and the frequency range of the measurements. Smaller diameter projectiles generally generate shorter pulses, increasing in this way the accuracy of the measuring technique. The useful frequency range reported, for sufficiently accurate results, for the larger diameter projectiles is 0 – 5 kHz.

Acknowledgment.

Acknowledgments are due to Dr J.J.Harrigan of the University of Aberdeen, UK, for his kind help with the experimental measurements, which were conducted at the University of Manchester, UK, and his overall supervision for the duration of the project.

Notation:

A – Cross-sectional area of the bar;	L – Bar length;
A_R – Number of active arms;	S – Gauge factor;
a – Bar radius;	t – Time;
$a(\omega)$ – Attenuation coefficient;	V_{in} – Particle velocity at the end of the input bar;
C – Stress wave velocity in the bars;	V_{out} – Particle velocity at the end of the output bar;
$C(\omega)$ – Phase velocity;	$\gamma(\omega)$ – Propagation coefficient;
d – Distance between the strain gauges and the free end of the bar;	δ – Complex change in the phase function of the frequency;
E – Young's modulus;	$\varepsilon_I(t), \varepsilon_R(t), \varepsilon_T(t)$ – Axial strains associated with the incident, reflected and transmitted waves respectively;
$E^*(\omega)$ – Complex Young's modulus;	$\tilde{\varepsilon}(x,\omega)$ – Fourier transform of the axial strain;
$F_{in}(t)$ – Force at the end of the input bar;	ρ – Density;
F_{out} – Force at the end of the output bar;	$\tilde{\sigma}(x,\omega)$ – Fourier transform of the axial Stress;
G – Gain setting of the amplifier;	ω – Angular frequency.
$k(\omega)$ – Wave number;	

Р Е З Ю М Е . Експериментально обчислено коефіцієнт поширення, який має зв'язок з дисперсією хвилі та коефіцієнтом затухання хвилі. Вказані дисперсія та коефіцієнт затухання отримані для матеріалу ПММА в залежності від частоти в серії дослідів з удару за допомогою стержня Гопкінсона. де використані кулі у вигляді сферичних підшипників різного діаметру. Застосовано метод корекції дисперсії хвиль із застосуванням швидкого перетворення Фур‘є щодо поздовжніх деформацій, який зв’язаний з падаючою та відбитою хвилями.

1. *Kolsky H*. An investigation of the mechanical properties of materials at very high rates of loading // Proc. Phys. Soc. – 1949. – **B 62**. – P. 670 – 700.
2. *Tamaogi T., Sogabe Y*. Examination of Validity for Viscoelastic Split Hopkinson Pressure Bar Method // SEM Annual Conference, Indianapolis, Indiana USA. – 2010. – P. 77 – 88.
3. *Zhao H, Gary G,* Crushing behaviour of aluminium honeycombs under impact loading // Int. J. Impact Eng. – 1998. – **21**. – P. 827 – 836.
4. *Zhao H., Gary G., Klepaczko J.R.* On the use of a viscoelastic Split Hopkinson Pressure Bar // Int. J. Impact Eng. – 1997. – **19**. – P. 319 – 330.
5. *Lifshitz J.M., Leber H.* Data processing in the split Hopkinson pressure bar tests // Int. J. Impact Eng. – 1994. – **15**. – P. 723 – 733.
6. *Zhao H., Gary G.* A three dimensional analytical solution of the longitudinal wave propagation in an infinite viscoelastic cylindrical bar. Application to experimental techniques // J. Phys. Solids. – 1995. – **43**. – P. 1335 – 1348.
7. *Bacon C*. An experimental method for considering dispersion and attenuation in a viscoelastic Hopkinson bar // Int. J. of Experimental Mechanics. – 1998. – **38**. – P. 242 – 249.
8. *Lundberg B., Blanc R.H.* Determination of Mechanical material properties from the Two-point Response of an Impacted Linearly Viscoelastic Rod Specimen // J. Sound Vibration. – 1988. – **126**. – P. 97 – 108.
9. *Bacon C.* Separation of waves propagating in an elastic or viscoelastic Hopkinson pressure bar with three-dimensional effects // Int. J. of Impact Eng. – 1998. – **22**. – P. 55 – 69.

From the Editorial Board: The article corresponds completely to submitted manuscript.

Поступила 05.02.2014 Утверждена в печать 19.02. 2015.